Carbohydrate Polymers 95 (2013) 50–56

Contents lists available at SciVerse ScienceDirect

Carbohydrate Polymers

journal homepage: www.elsevier.com/locate/carbpol

Two-step method for encapsulation of oregano essential oil in chitosan nanoparticles: Preparation, characterization and *in vitro* release study

Seyed Fakhreddin Hosseini[a], Mojgan Zandi[b,*], Masoud Rezaei[a], Farhid Farahmandghavi[c]

[a] Department of Fisheries, Faculty of Marine Sciences, Tarbiat Modares University, P.O. Box 46414-356, Noor, Iran
[b] Department of Biomaterials, Iran Polymer and Petrochemical Institute, P.O. Box 14965/115, Tehran, Iran
[c] Department of Novel Drug Delivery Systems, Iran Polymer and Petrochemical Institute, P.O. Box 14965/115, Tehran, Iran

ARTICLE INFO

Article history:
Received 26 November 2012
Received in revised form 30 January 2013
Accepted 16 February 2013
Available online 26 February 2013

Keywords:
Chitosan
Encapsulation
In vitro release
Nanoparticles
Oregano essential oil

ABSTRACT

In this study, oregano essential oil (OEO) has been encapsulated in chitosan nanoparticles by a two-step method, *i.e.*, oil-in-water emulsion and ionic gelation of chitosan with sodium tripolyphosphate (TPP). The success of OEO encapsulation was confirmed by Fourier transform infrared (FT-IR) spectroscopy, UV–vis spectrophotometry, thermogravimetric analysis (TGA) and X-ray diffraction (XRD) techniques. The obtained nanoparticles exhibited a regular distribution and spherical shape with size range of 40–80 nm as observed by scanning electron microscopy (SEM) and atomic force microscopy (AFM). As determined by TGA technique, the encapsulation efficiency (EE) and loading capacity (LC) of OEO-loaded chitosan nanoparticles were about 21–47% and 3–8%, respectively, when the initial OEO content was 0.1–0.8 g/g chitosan. *In vitro* release studies showed an initial burst effect and followed by a slow drug release.

1. Introduction

Essential oils (EOs) are aromatic and volatile oily liquids obtained from plants. They are normally formed in special cells or groups of cells, found in leaves and stems, and commonly concentrated in one particular region such as leaves, bark or fruit (Oussalah, Caillet, Saucier, & Lacroix, 2006). EOs extracted from plants or spices are rich sources of biologically active compounds such as terpenoids and phenolic acids. The antibacterial and antifungal activities of EOs have long been recognized (Burt, 2004; Nychas, 1995), but the food industry has recently been paying more attention to their application as natural antimicrobials (Plooy, Regnier, & Combrinck, 2009). Within a great variety of EOs, oregano essential oil (OEO) extracted from *Origanum vulgare* L. is well known for its antioxidative and antimicrobial activity (Botsoglou, Grigoropoulou, Botsoglou, Govaris, & Papageorgiou, 2003). These activities are mainly due to the two phenols, carvacrol and thymol (major components of oregano essential oil) and the monoterpene hydrocarbons *p*-cymene and γ-terpinene (Baydar, Sagdic, Ozkan, & Karadogan, 2004) which present at lower concentration (Juliano, Mattana, & Usai, 2000).

However, like other EOs, OEO are volatile compound which easily evaporates and/or decomposes during food processing, drug formulation, and preparation of antimicrobial film, *etc.*, owing to direct exposure to heat, pressure, light or oxygen. In order to overcome the susceptibility and improve the stability of bioactive compounds during processing and storage, the emerging technology of nano-encapsulation has been recently applied in food and nutraceutical industries. Nanoencapsulation of bioactive compounds represents a viable and efficient approach to increase the physical stability of the active substances, protect them from the interactions with the food ingredients and enhance their bioactivity, because of the subcellular size (Donsì, Annunziata, Sessa, & Ferrari, 2011). In other words, encapsulation can reduce the loss of activity of the active compounds. In the case of antimicrobials, the nano-level encapsulation can increase the concentration of the bioactive compounds in food areas where microorganisms are preferably located, for example water-rich phases or liquid–solid interfaces (Weiss, Gaysinksy, Davidson, & McClements, 2009).

In the recent years, there has been considerable interest in developing biodegradable nanoparticles as effective lipophilic bioactive food components delivery systems. Chitosan is receiving a lot of interest in the encapsulation of bioactive compounds due to its biocompatibility, low toxicity and biodegradability (Donsì et al., 2011; Harris, Lecumberri, Mateos-Aparicio, Mengíbar, & Heras,

* Corresponding author. Tel.: +98 2148662422; fax: +98 2144580023.
E-mail address: m.zandi@ippi.ac.ir (M. Zandi).

0144-8617/$ – see front matter © 2013 Elsevier Ltd. All rights reserved.
http://dx.doi.org/10.1016/j.carbpol.2013.02.031

2011; Hu et al., 2008; Luo, Zhang, Whent, Yu, & Wang, 2011; Muzzarelli, 2010). Among variety of methods developed to prepare chitosan nanoparticles, ionic gelation technique has attracted considerable attention due to this process is non-toxic, organic solvent free, convenient and controllable (Agnihotri, Mallikarjuna, & Aminabhavi, 2004). Ionic gelation technique is based on the electrostatic interaction between the positively charged primary amino groups of chitosan and the negatively charged groups of polyanion, such as sodium tripolyphosphate (TPP) (Calvo, Remũnán-López, & Vila-Jato Alonso, 1997; Dyer et al., 2002; Yang et al., 2011). The chitosan–TPP nanoparticles, composed of food-safe ingredients, has shown its capacity for the encapsulation and delivery of proteins (Avadi et al., 2009; Xu & Du, 2003), genes (Csaba, Köping-Höggård, & Alonso, 2009; Gan, Wang, & McCarron, 2005), hydrophilic and hydrophobic drugs (Ajun, Yan, Li, & Huili, 2009; Trapani et al., 2011; Wang et al., 2006), vitamins (Luo et al., 2011; Yoksan, Jirawutthiwongchai, & Arpo, 2010), and polyphenolic compounds (Bao, Xu, & Wang, 2009; Dudhani & Kosaraju, 2010; Keawchaoon & Yoksan, 2011). Keawchaoon and Yoksan (2011) revealed that the encapsulation of essential oil-derived bioactive compounds such as carvacrol into chitosan–tripolyphosphate particles could extend its shelf life and retain its functional properties. Generally, EOs possessing the strongest antibacterial properties are those that contain phenolic compounds such as carvacrol, eugenol, and thymol (Hirasa & Takemasa, 1998; Rota, Carraminana, Burillo, & Herrera, 2004). To our knowledge, the loading of OEO into chitosan particles at a nanolevel size has not been elucidated.

The present research thus focused on the fabrication and characterization of chitosan–TPP nanoparticles loaded with OEO by a two-step process: oil-in-water (o/w) emulsification, and ionic gelation. We also clarified the successful encapsulation by UV–vis spectrophotometry, FT-IR spectroscopy, TGA and XRD techniques, and determined the shape, morphology and mean particle size by SEM, AFM, and laser light scattering (LLS). The effects of initial OEO content on loading capacity (LC), encapsulation efficiency (EE), and mean particles size were also investigated. In addition, the release profiles of OEO from chitosan nanoparticles were investigated.

2. Materials and methods

2.1. Materials

Medium molecular weight chitosan (75–85% degree of deacetylation, CAS # 9012-76-4), TPP (CAS # 7758-29-4) and Tween 80 (CAS # 9005-65-6) were purchased from Sigma–Aldrich (St. Louis, MO, USA). Acetic acid (CAS # 64-19-7) was supplied by Merck Chemicals Co. (Darmstadt, Germany). OEO (100% pure, CAS # 8007-11-2) was obtained from New Directions Aromatics Inc. (Hampshire, UK). All chemicals were used as received without further purification.

2.2. Preparation of OEO-loaded chitosan particles

OEO-loaded chitosan nanoparticles were prepared according to a method modified from the ones described by Calvo et al. (1997) and Yoksan et al. (2010). Briefly, aqueous and oil phase solutions were produced. Chitosan solution (1% (w/v)) was prepared by agitating chitosan in an aqueous acetic acid solution (1% (v/v)) at ambient temperature (23–25 °C) overnight. The mixture was then centrifuged using a laboratory centrifuges (SIGMA 2-16KC, Germany) for 30 min at 9000 rpm; the supernatant was removed then and filtered through 1 μm pore size filters. Tween 80 (HLB 15.9, 0.45 g) was then added as a surfactant to the solution (40 mL) and stirred at 45 °C for 2 h to obtain a homogeneous mixture.

OEO (0.04, 0.08, 0.16 and 0.32 g) was dissolved separately in CH_2Cl_2 (4 mL) and then this oil phase is gradually dropped into the aqueous chitosan solution (40 mL) during homogenization (Ultra-Turrax T25 basic, IKA, Germany) at a speed of 13,000 rpm for 10 min under an ice-bath condition to obtain an oil-in-water emulsion. TPP solution (0.4% (w/v), 40 mL) was then added drop wise into the agitated emulsion. Agitation was continuously performed for 40 min. The formed particles were collected by centrifugation at 9000 × *g* for 30 min at 4 °C, and subsequently washed several times with deionized water. Finally, ultrasonication was performed by a sonicatior (Bandelin sonopuls HD3200, KE 76 probe, Germany) in an ice bath for 4 min with a sequence of 0.7 s of sonication and 0.3 s of rest, resulting in a homogeneous suspension. The suspensions were immediately freeze-dried at −35 °C for 72 h using Freeze Dryer (GAMMA 1-16 LSC, UK). Both chitosan nanoparticles and supernatant were stored at 4 °C until further analysis. Weight ratios of chitosan to oregano essential oils (Chitosan: OEO) of 1:0.1, 1:0.2, 1:0.4 and 1:0.8 were used for the present study.

2.3. Particle size and morphology of nanoparticles

Measurement of mean particle size of freshly prepared nanoparticles was determined by laser light scattering (SEMATECH, SEM-633, France) with 633 nm wavelength. Triplicate samples were analyzed and mean value was reported.

The morphology of the freeze-dried nanoparticles was studied by scanning electron microscopy (SEM) (VEGA II, TESCAN, Czech Republic). The frozen dried nanoparticles (1 mg) were dispersed in deionized water (20 mL) and sonicated for 4 min. One drop of the dispersion containing chitosan nanoparticles (loaded or unloaded with OEO) was placed on a glass plate and dried at room temperature. The dried nanoparticles were then coated with gold metal under high vacuum and then examined. Representative SEM images were reported.

Atomic force microscope (DualScope™ DS95-50, DME, Denmark) was used for morphological characterization and particle size and size distribution of both chitosan nanoparticles and OEO-loaded chitosan nanoparticles. A drop of diluted nanoparticle suspension (0.05 mg/mL) was deposited on the freshly cleaved clean glass surface, spread and dried at room temperature. The image measurement was performed in tapping mode using silicon probe cantilever of 230 μm length, resonance frequency of 150–190 kHz, spring constant of 20–60 N/m and nominal, 5–10 nm tip radius of curvature. The scan rate was used as 1 Hz. A minimum of 10 images from each sample were analyzed to assure reproducible results.

2.4. Instrumental analyses

FTIR analyses for pure chitosan, pure OEO and chitosan nanoparticles (loaded or unloaded with OEO) were recorded from wave number 400–4000 cm^{-1} by a Bruker Equinox 55 spectrometer (Equinox 55 Bruker Banner Lane, Coventry, Germany). Samples were prepared by grinding the dried nanoparticles with KBr and pressing them to form disks. For each spectrum, 16 scans at a resolution of 4 cm^{-1} were obtained.

TGA analysis was performed with a Perkin-Elmer PYRIS I Thermogravimetric Analyzer (USA). Each freeze-dried sample (10–15 mg) was placed in the TGA furnace and the measurements were carried out under nitrogen atmosphere with a heating rate of 10 °C/min from 25 to 600 °C.

XRD patterns were recorded over a 2θ range of 5–50° using a X-ray diffractometer (Siemens, model D5000) with a step angle of 0.04°/min.

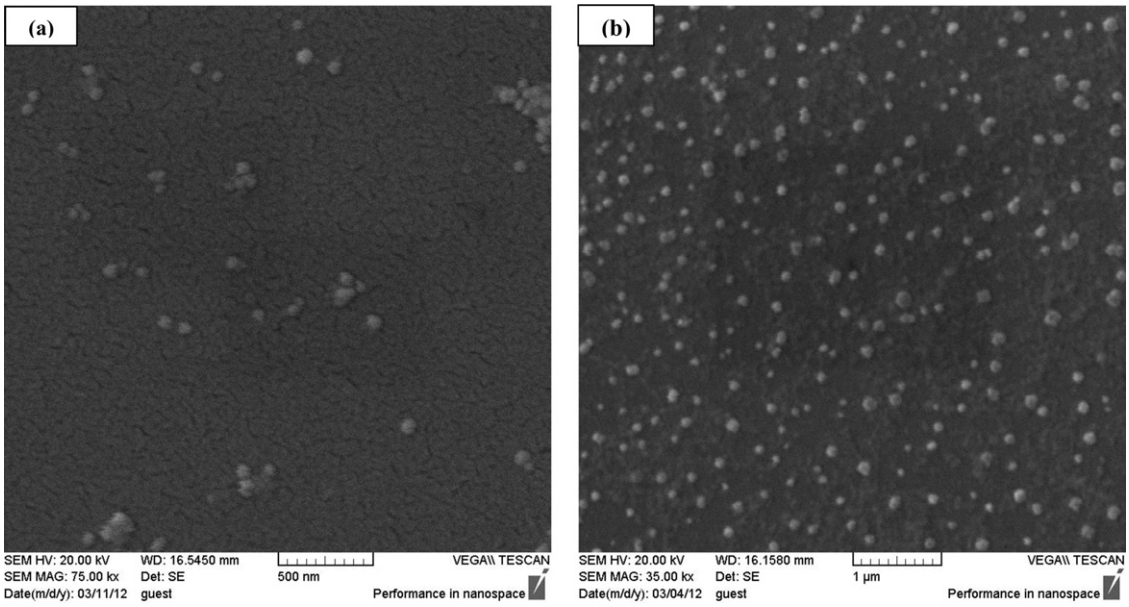

Fig. 1. SEM images of (a) chitosan nanoparticles and (b) OEO-loaded chitosan nanoparticles prepared using an initial weight ratio of chitosan to OEO of 1:0.4.

2.5. Determination of encapsulation efficiency and loading capacity

The content of OEO-loaded in chitosan nanoparticles was determined by UV–vis spectrophotometry and TGA/DTG (derivative thermal gravimetric) techniques. For UV–vis spectrophotometry, OEO-loaded nanoparticles (10 mg) were taken into aqueous hydrochloric acid solution (2 M, 4 mL) and boiled at 95 °C for 30 min. After cooling down, ethanol (2 mL) was subsequently added to the mixture. The mixture was centrifuged at 9000 rpm for 5 min at 25 °C (Keawchaoon & Yoksan, 2011). The supernatant was collected and the content of OEO measured using UV-vis spectrophotometer (Model 1650-PC, Shimadzu, Kyoto, Japan) at a wavelength of 275 nm (Parris, Cooke, & Hicks, 2005). The amount of OEO was calculated by appropriate calibration curve of free OEO in ethanol (R^2 = 0.999). A blank sample was made from chitosan nanoparticles without loaded OEO but treated similarly as the OEO-loaded chitosan nanoparticles. Each batch samples were measured in triplicate. The encapsulation efficiency (EE) and loading capacity (LC) of OEO were calculated from Eqs. (1) and (2) respectively:

$$\text{EE}\,(\%) = \frac{\text{Total amount of loaded OEO}}{\text{Initial amount of OEO}} \times 100 \quad (1)$$

$$\text{LC}\,(\%) = \frac{\text{Total amount of loaded OEO}}{\text{Weight of nanoparticles after freeze drying}} \times 100 \quad (2)$$

2.6. In vitro release studies

Freeze-dried OEO-loaded chitosan nanoparticles (20 mg) were placed in a microtube containing 5 mL of 60% phosphate buffer saline (pH 7.4) + 40% ethanol and incubated at ambient temperature under gentle agitation. At specific time intervals, samples were centrifuged at 9000 rpm for 5 min at 25 °C; then a specific volume of supernatant was sucked out for analysis, and was replaced with an equivalent volume of fresh media. To calculate the total cumulative amount of OEO released loaded chitosan nanoparticles, OEO concentration (ppm) in the release medium was measured at sampling time intervals by a UV–vis spectrophotometer at 275 nm and converted to the released amount (μg) considering the volume of the release medium (mL). Cumulative percentage of OEO released was obtained by dividing the cumulative amount of OEO released at each sampling time point (M_t) to the initial weight of the OEO-loaded in the sample (M_0), *i.e.*:

$$\text{Cumulative release percentage} = \sum_{t=0}^{t} \frac{M_t}{M_0} \times 100 \quad (3)$$

3. Results and discussion

3.1. Shape and size of OEO-loaded chitosan nanoparticles

The morphology of the particles was observed by SEM. The SEM images of the chitosan nanoparticles and OEO-loaded chitosan nanoparticles demonstrate regular distribution and spherical shape that appear to be well separated and stable over the steps of the preparation process (Fig. 1(a) and (b)). AFM imaging is an effective method to provide the surface morphology and more accurate size and size distribution. AFM images also confirmed the spherical shape and nanosize structure of chitosan nanoparticles and OEO-loaded chitosan nanoparticles (Fig. 2(a) and (b)). The size distribution obtained by AFM indicated that most of chitosan nanoparticles and OEO-loaded chitosan nanoparticles were distributed between the ranges of 40 and 80 nm. However, the size of the chitosan nanoparticles is smaller compared to the OEO-loaded nanoparticles. The increase of nanoparticle size is due to loading of OEO on chitosan nanoparticles. Laser light scattering (LLS) technique was also applied to investigate the average size of the particles. Table 1 shows that chitosan nanoparticles possessed an average diameter of 281.5 nm. OEO-loaded chitosan particles showed an average diameter in the range of 309.8–402.2 nm. Our results indicated that the mean particle size increased as a function of initial OEO content (Table 1), which is concurrent to the findings of Keawchaoon and Yoksan (2011). As compared with AFM results, the larger diameter of chitosan nanoparticles (loaded or unloaded with OEO) might be a result of the swelling of the chitosan layer surrounding the individual particles, and/or the aggregation of single particles while dispersed in water (Yoksan et al., 2010).

3.2. FTIR characterization

Fig. 3 shows FTIR spectra of chitosan powder, chitosan nanoparticles, OEO and OEO-loaded chitosan nanoparticles. In general,

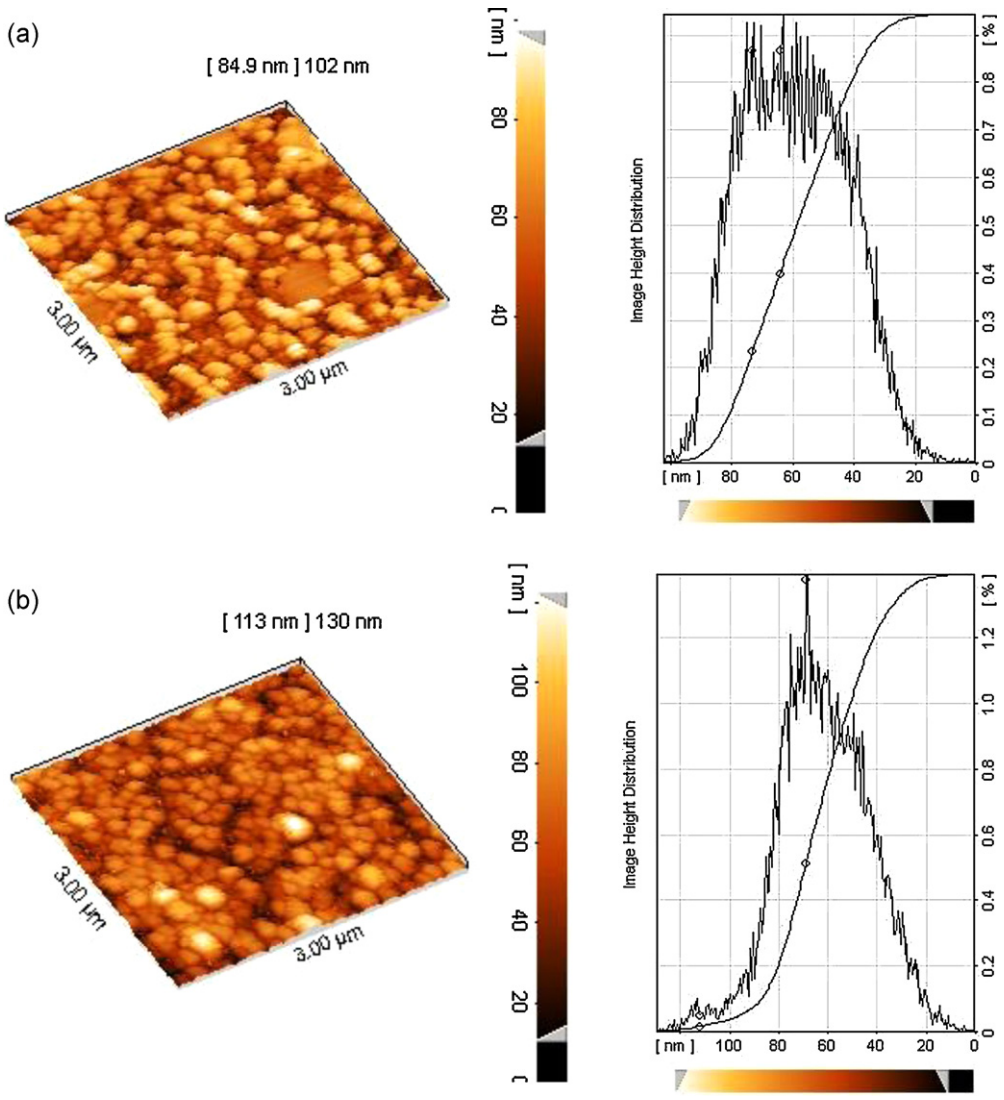

Fig. 2. AFM images (3D) and size distribution obtained from the height of (a) chitosan nanoparticles and (b) OEO-loaded chitosan nanoparticles prepared using an initial weight ratio of chitosan to OEO of 1:0.4.

chitosan powder show characteristic peaks at 3433 (—OH and —NH_2 stretching), 2920 (—CH stretching), 1647 (amide I), 1088 (C—O—C stretching) and 591 cm^{-1} (pyranoside ring stretching vibration) (Fig. 3(a)). For chitosan nanoparticles (Fig. 3(b)), the peak of amide I (—NH_2 bending) shifted from 1647 to 1651 cm^{-1}, and new peaks appeared at 1238 (C—O—C stretch) and 1555 cm^{-1} (amide II), implying the complex formation *via* electrostatic interaction between NH^{3+} groups of chitosan and phosphoric groups of TPP within the nanoparticles (Yoksan et al., 2010; Jingou et al., 2011). Pure OEO spectra shows sharp characteristic peaks at 2959 (—CH stretching), 1589 (N—H bending), 1458 (CH_2 bending), 1253 (C—O—C stretching), 1117 (C—O—C stretching) and 937 cm^{-1} (C—H bending) (Fig. 3(c)). All the above characteristic peaks appear in the spectra of OEO-loaded chitosan nanoparticles at the same wave number indicating no modification or interaction between the OEO and chitosan nanoparticles (Fig. 3(d)). Moreover, in comparison with the FTIR spectrum of chitosan nanoparticles, the addition of OEO resulted in a markedly increased in intensity of the CH stretching peak at 2867–2955 cm^{-1}, indicating an increase in the content of ester groups, which might come from OEO molecules

Table 1
Encapsulation efficiency (EE%) and loading capacity (LC%) of OEO in OEO-loaded chitosan nanoparticles determined by UV–vis spectrophotometry and TGA technique, and mean particle size of chitosan nanoparticles and OEO-loaded chitosan nanoparticles.

Chitosan:OEO mass ratio (w/w)	UV–vis spectrophotometry		TGA		Mean particle size (nm)
	EE (%)	LC (%)	EE (%)	LC (%)	
1:0	0	0	0	0	281.5 ± 24.1
1:0.1	24.72 ± 4.39	1.32 ± 0.19	47.69	3.08	309.8 ± 8.3
1:0.2	14.68 ± 1.1	1.75 ± 0.13	39.94	4.77	331.4 ± 10.1
1:0.4	8.53 ± 0.94	2.03 ± 0.22	26.85	6.40	366.6 ± 21.5
1:0.8	5.45 ± 0.45	2.12 ± 0.17	21.09	8.21	402.2 ± 10.7

Results were reported as mean ± SD, $n = 3$.

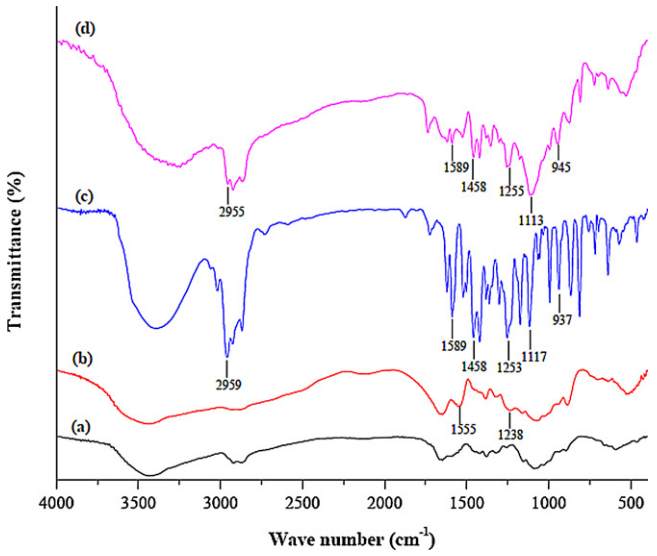

Fig. 3. FTIR spectra of (a) chitosan powder, (b) chitosan nanoparticles, (c) OEO and (d) OEO-loaded chitosan nanoparticles with chitosan to OEO weight ratio of 1:0.4.

(Fig. 3(d)). The results indicate that OEO might be encapsulated into the chitosan nanoparticles.

3.3. Thermal properties

TGA is a useful technique to study the weight change of a sample as a function of temperature, and to assess the thermal stability of a sample. As shown in the TGA thermograms, OEO possessed only one step of weight loss (Fig. 4A(a)), while chitosan nanoparticles and OEO-loaded chitosan nanoparticles showed two (Fig. 4A(b)) and three steps of weight loss (Fig. 4A(c–f)), respectively. The first step of weight loss from 50 to 110 °C was attributed to the loss of adsorbed and bound water. The second step from 190 to 330 °C was assigned to dehydration of the saccharide rings, depolymerization and decomposition of the acetylated and deacetylated units of the polymer (Peniche, Zaldivar, Bulay, & Roman, 1993). The temperatures corresponding to the maximum slopes of each weight change step are clearly observed when the first derivative of the TGA curve with respect to temperature, the so-called derivative thermogravimetry (DTG) thermogram, is plotted (Fig. 4B). The temperatures which give the highest rate of weight loss at each step (*i.e.*, peaks in the DTG thermogram) are usually considered as degradation temperatures (T_d) of components in the material (Yoksan et al., 2010). OEO showed one-step mass loss starting at 171 °C (peak at 195 °C) (Fig. 4B(a)). From DTG thermograms, chitosan nanoparticles exhibited two-step degradation, at 246.3 and 330 °C-which might be the T_d of free chitosan and chitosan cross-linked with TPP, respectively (Fig. 4B(b)). By loading of OEO, the particles showed new T_d ranging from 338 to 358 °C (Fig. 4B(c–f)), which could be ascribed to the T_d of encapsulated OEO. The percent weight loss at this temperature range was thus used to compute the amount of loaded OEO (Section 3.5). This finding is in agreement with results reported by Keawchaoon and Yoksan (2011). These authors represented that the encapsulated carvacrol in chitosan particles decomposed at higher temperature (340.6 °C) than free carvacrol (186.4 °C), reflecting the improved thermal stability of carvacrol by encapsulation.

3.4. Crystallographic assay

Crystallographic structure of chitosan powder, chitosan nanoparticles and the OEO-loaded chitosan nanoparticles were

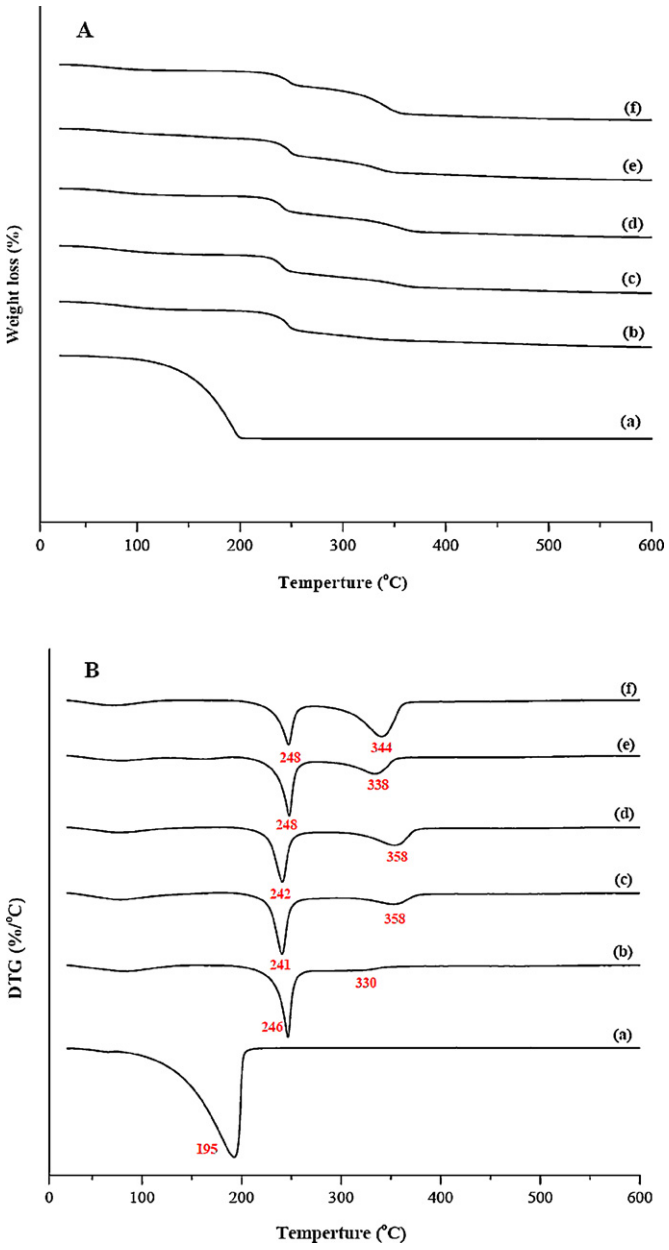

Fig. 4. (A) TGA and (B) DTG thermograms of (a) OEO, (b) chitosan nanoparticles and (c)–(f) OEO-loaded chitosan nanoparticles prepared using different initial weight ratios of chitosan to OEO: (c) 1:0.1, (d) 1:0.2, (e) 1:0.4, and (f) 1:0.8.

determined by XRD and are presented in Fig. 5. chitosan exhibits one characteristic peak at 2θ of 25° (Fig. 5(a)), indicating the high degree of crystallinity (Ali, Rajendran, & Joshi, 2011; Jingou et al., 2011). After ionic cross-linking with TPP, no peak is found in the diffractograms of chitosan nanoparticles, reflecting the destruction of the native chitosan packing structure (Yoksan et al., 2010) (Fig. 5(b)). It is well-known that the width of X-ray diffraction peak is related to the size of crystallite, the broadened peak usually results from imperfect crystal (Jingou et al., 2011). So the broad peak of chitosan nanoparticles may be caused by the cross-linking reaction between chitosan and TPP, which may destroy the crystalline structure of chitosan (Rokhade et al., 2006). Chitosan nanoparticles are comprised of a dense network structure of interpenetrating polymer chains crosslinked to each other by TPP counterions (Tang, Huang & Lim, 2003). The XRD implicated greater disarray in chain alignment in the nanoparticles after crosslinks (Qi, Xu, Jiang, Hu, & Zou, 2004). As compared with

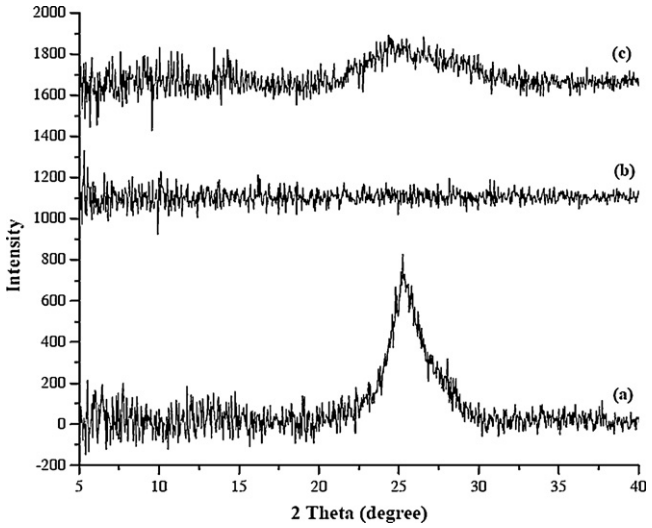

Fig. 5. XRD patterns of (a) chitosan powder, (b) chitosan nanoparticles and (c) OEO-loaded chitosan nanoparticles.

chitosan nanoparticles, in diffraction spectrum of OEO-loaded chitosan nanoparticles the characteristic peak at 2θ of 24° confirming the presence of OEO within chitosan nanoparticles (Fig. 5(c)). This implied that the incorporation of OEO resulted in a change in the chitosan–TPP packing structure.

3.5. Encapsulation efficiency and loading capacity

The percentage of EE and LC of different formulations were demonstrated in Table 1. The amount of loaded OEO was determined using UV–vis spectrophotometry from the absorbance at 275 nm. TGA technique was also applied for quantitative analysis from the mass loss at the temperature of 338–358 °C (Fig. 4A(c–f)). The loading capacity (LC) and encapsulation efficiency (EE) were then calculated using Eqs. (1) and (2), respectively, and tabulated in Table 1. From UV–vis spectrophotometry results, EE% of OEO ranged from 5.45% to 24.72% (Table 1). With increasing initial OEO content, EE tended to decrease. However, maximum EE value was obtained for the sample prepared using the weight ratio of chitosan to OEO of 1:0.1 (24.72%). The decrease of EE for the samples prepared using higher initial weight ratio of chitosan to OEO might be explained due to the saturation of OEO loading into chitosan nanoparticles. This finding was in agreement with previous reports (Ajun et al., 2009; Yoksan et al., 2010). The LC% of OEO was in the range of 1.32–2.12%, as determined from UV–vis spectrophotometry experiments, when the initial OEO content ranged from 0.1 to 0.8 g/g chitosan (Table 1). The LC% increased as a function of initial OEO content. This result was in agreement with the findings regarding the loading of carvacrol into chitosan–TPP nanoparticles, which have been reported by Keawchaoon and Yoksan (2011).

Information obtained from TGA thermograms was also used to determine the content of OEO-loaded in chitosan nanoparticles. Based on this result, the EE% and LC% of OEO were in a range of 21.09–47.69% and 3.08–8.21%, respectively (Table 1). This observation supported the results from UV–vis spectrophotometry, which LC increased with increasing OEO content, whereas EE decreased. The augmentation of LC and reduction of EE as a function of initial drug content corresponded to previous literature related to the loading of ascorbyl palmitate into chitosan–TPP nanoparticles (Yoksan et al., 2010).

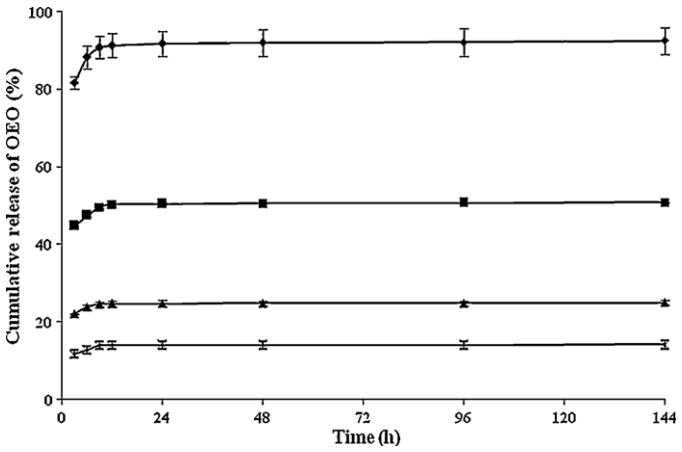

Fig. 6. *In vitro* release profiles of OEO from chitosan nanoparticles prepared using different weight ratio of chitosan to OEO: (♦) 1:0.1, (■) 1: 0.2, (▲) 1:0.4 and (×) 1:0.8. Values were expressed as mean ± standard deviation ($n = 3$).

3.6. In vitro release study

The *in vitro* release profiles of OEO from the nanoparticles, prepared using a different weight ratio of chitosan to OEO were shown in Fig. 6. The amount of OEO released at different times was measured at 275 nm. Drug or oil release from nanoparticles and microparticles takes place by several mechanisms including surface erosion, disintegration, diffusion and desorption (Hariharan et al., 2006). The *in vitro* release profile of OEO from chitosan nanoparticles can be described as a two-step biphasic process, *i.e.*, an initial burst release followed by subsequent slower release. The initial burst release was attributed to the OEO molecules adsorbed on the surface of the particles and oil entrapped near the surface, as the dissolution rate of the polymer near the surface is high, the amount of drug released will be also high (Anitha et al., 2011). Fig. 6 shows the release profile as a function of OEO concentration, which was found to be concentration dependent. At low concentration of OEO (0.1 g/g chitosan), burst effect occurred within 3 h and about 82% encapsulated OEO was released from the nanoparticles. This could be mainly attributed to the particle size of this formulation. chitosan nanoparticles with smaller particle size would have greater surface-to-volume ratio, thus may result in fast release of OEO adsorbed on the surface. Similar results with an initial release of 85% encapsulated α-tocopherol were reported with chitosan nanoparticles coated with zein and later followed slow release at a constant but different rate (Luo et al., 2011). As OEO concentration increased, the burst effect was dramatically alleviated and the accumulative release after 3 h was reduced from 82% to 12%, as OEO concentration reached 0.8 g/g chitosan. In the second stage, the release rate was relatively slow, or we could say that the release of OEO reached plateau at this stage (Figs. 6). This might be due to the diffusion of the OEO dispersed into the polymer matrix as the dominant mechanism. This stage has slower rate and thus resulting in nearly no additional release of OEO at this stage. Further release of OEO required the swelling and degradation of the compact chitosan–TPP nanoparticles. Hence, the results indicate that the chitosan–TPP nanosystem is suitable for controlling the release of OEO.

4. Conclusions

OEO-loaded chitosan nanoparticles were successfully prepared by two-step method, *i.e.*, the formation of an oil-in-water emulsion and the ionic gelation of emulsion droplets, as confirmed by instrumental analytical techniques (FTIR, TGA/DTG and XRD). The

particles were spherical in shape with size range 40–80 nm. By increasing the weight ratio of OEO to chitosan, LC% is increased, while EE% is decreased. The *in vitro* release studies indicated that the content of OEO in the nanoparticles influenced its release rate from the chitosan nanoparticles. In future studies, it would therefore be useful to examine the performance of chitosan-based nanoparticles for encapsulation of other essential oils by this two-step method.

Acknowledgments

This study was carried out under Ph.D. student research fund for the Tarbiat Modares University and was sponsored by Iran National Science Foundation under Project 2011-90000234.

References

Agnihotri, S. A., Mallikarjuna, N. N., & Aminabhavi, T. M. (2004). Recent advances on chitosan-based micro and nanoparticles in drug delivery. *Journal of Controlled Release*, *100*, 5–28.

Ajun, W., Yan, S., Li, G., & Huili, L. (2009). Preparation of aspirin and probucol in combination loaded chitosan nanoparticles and *in vitro* release study. *Carbohydrate Polymers*, *75*, 566–574.

Ali, S. W., Rajendran, S., & Joshi, M. (2011). Synthesis and characterization of chitosan and silver loaded chitosan nanoparticles for bioactive polyester. *Carbohydrate Polymers*, *83*, 438–446.

Anitha, A., Deepagan, V. G., Divya Rani, V. V., Menon, D., Nair, S. V., & Jayakumar, R. (2011). Preparation, characterization in vitro drug release and biological studies of curcumin loaded dextran sulphate–chitosan nanoparticles. *Carbohydrate Polymers*, *84*, 1158–1164.

Avadi, M. R., Sadeghi, A. M. M., Mohammadpour, N., Abedin, S., Atyabi, F., Dinarvand, R., et al. (2009). Preparation and characterization of insulin nanoparticles using chitosan and Arabic gum with ionic gelation method. *Nanomedicine: Nanotechnology, Biology and Medicine*, *6*, 58–63.

Bao, S., Xu, S., & Wang, Z. (2009). Antioxidant activity and properties of gelatin films incorporated with tea polyphenol-loaded chitosan nanoparticles. *Journal of the Science of Food and Agriculture*, *89*, 2692–2700.

Baydar, H., Sagdic, O., Ozkan, G., & Karadogan, T. (2004). Antibacterial activity and composition of essential oils from *Oreganum Thymbra* and *Satureja* species with commercial importance in Turkey. *Food Control*, *15*, 169–172.

Botsoglou, N. A., Grigoropoulou, S. M., Botsoglou, E., Govaris, A., & Papageorgiou, G. (2003). The effects of dietary oregano essential oil and a-tocopheryl acetate on lipid oxidation in raw and cooked turkey during refrigerated storage. *Meat Science*, *65*, 1193–1200.

Burt, S. (2004). Essential oils: Their antibacterial properties and potential applications in foods: A review. *International Journal of Food Microbiology*, *94*, 223–253.

Calvo, P., Remũnán-López, C., Vila-Jato, J. L., & Alonso, M. J. (1997). Novel hydrophilic chitosan–polyethylene oxide nanoparticles as protein carrier. *Journal of Applied Polymer Science*, *63*, 125–132.

Csaba, N., Köping-Höggård, M., & Alonso, M. J. (2009). Ionically crosslinked chitosan/tripolyphosphate nanoparticles for oligonucleotide and plasmid DNA delivery. *International Journal of Pharmaceutics*, *382*, 205–214.

Donsì, F., Annunziata, M., Sessa, M., & Ferrari, G. (2011). Nanoencapsulation of essential oils to enhance their antimicrobial activity in foods. *LWT: Food Science and Technology*, *44*, 1908–1914.

Dudhani, A. R., & Kosaraju, S. L. (2010). Bioadhesive chitosan nanoparticles: Preparation and characterization. *Carbohydrate Polymers*, *81*, 243–251.

Du Plooy, W., Regnier, T., & Combrinck, S. (2009). Essential oil amended coatings as alternatives to synthetic fungicides in citrus postharvest management. *Postharvest Biology and Technology*, *53*, 117–122.

Dyer, A. M., Hinchcliffe, M., Watts, P., Castile, J., Jabbal-Gill, I., Nankervis, R., et al. (2002). Nasal delivery of insulin using novel chitosan based formulations: A comparative study in two animal models between simple chitosan formulations and chitosan nanoparticles. *Pharmaceutical Research*, *19*, 998–1008.

Gan, Q., Wang, T., & McCarron, P. (2005). Modulation of surface charge particle size and morphological properties of chitosan–TPP nanoparticles intended for gene delivery. *Colloids and Surfaces B: Biointerfaces*, *44*, 65–73.

Hariharan, S., Bhardwaj, V., Bala, I., Sitterberg, J., Bakowsky, U., & Ravi Kumar, M. N. (2006). Design of estradiol loaded PLGA nanoparticulate formulations: A potential oral delivery system for hormone therapy. *Pharmaceutical Research*, *23*, 184–195.

Harris, R., Lecumberri, E., Mateos-Aparicio, I., Mengíbar, M., & Heras, A. (2011). Chitosan nanoparticles and microspheres for the encapsulation of natural antioxidants extracted from *Ilex paraguariensis*. *Carbohydrate Polymers*, *84*, 803–806.

Hirasa, K., & Takemasa, M. (1998). Antimicrobial and antioxidant properties of spices. In K. Hirasa, & M. Takemasa (Eds.), *Spice science and technology* (pp. 163–200). New York: Marcel Dekker Inc.

Hu, B., Pan, C., Sun, Y., Hou, Z., Ye, H., Hu, B., et al. (2008). Optimization of fabrication parameters to produce chitosan–tripolyphosphate nanoparticles for delivery of tea catechins. *Journal of Agricultural and Food Chemistry*, *56*, 7451–7458.

Jingou, J., Shilei, H., Weiqi, L., Danjun, W., Tengfei, W., & Yi, X. (2011). Preparation characterization of hydrophilic and hydrophobic drug in combine loaded chitosan/cyclodextrin nanoparticles and *in vitro* release study. *Colloids and Surfaces B: Biointerfaces*, *83*, 103–107.

Juliano, C., Mattana, A., & Usai, M. (2000). Composition and *in vitro* antimicrobial activity of the essential oil of *Thymus herba-barona* Loisel growing wild in Sardinia. *Journal of Essential Oil Research*, *12*, 516–522.

Keawchaoon, L., & Yoksan, R. (2011). Preparation characterization and *in vitro* release study of carvacrol-loaded chitosan nanoparticles. *Colloids and Surfaces B: Biointerfaces*, *84*, 163–171.

Luo, Y., Zhang, B., Whent, M., Yu, L., & Wang, Q. (2011). Preparation and characterization of zein/chitosan complex for encapsulation of α-tocopherol and its *in vitro* controlled release study. *Colloids and Surfaces B: Biointerfaces*, *85*, 145–152.

Muzzarelli, R. A. A. (2010). Chitins and chitosans as immunoadjuvants and non-allergenic drug carriers. *Marine Drugs*, *8*, 292–312.

Nychas, G. J. E. (1995). Natural antimicrobials from plants. In G. W. Gould (Ed.), *New methods of food preservation* (pp. 58–89). London: Blackie Academic Professional.

Oussalah, M., Caillet, S., Saucier, L., & Lacroix, M. (2006). Inhibitory effects of selected plant essential oils on the growth of four pathogenic bacteria: *E. coli* O157:H7, *Salmonella Typhimurium*, *Staphylococcus aureus* and *Listeria monocytogenes*. *Food Control*, *18*, 414–420.

Parris, N., Cooke, P. H., & Hicks, K. B. (2005). Encapsulation of essential oils in zein nanospherical particles. *Journal of Agricultural and Food Chemistry*, *53*, 4788–4792.

Peniche, C., Zaldivar, D., Bulay, A., & Roman, J. S. (1993). Study of the thermal-degradation of poly (furfuryl methacrylate) by thermogravimetry. *Polymer Degradation and Stability*, *40*, 287–295.

Qi, L., Xu, Z., Jiang, X., Hu, C., & Zou, X. (2004). Preparation and antibacterial activity of chitosan nanoparticles. *Carbohydrate Research*, *339*, 2693–2700.

Rokhade, A. P., Agnihotri, S. A., Patil, S. A., Mallikarjuna, N. N., Kulkarni, P. V., & Aminabhavi, T. M. (2006). Semi-interpenetrating polymer network microspheres of gelatin and sodium carboxymethyl cellulose for controlled release of ketorolac tromethamine. *Carbohydrate Polymers*, *65*, 243–252.

Rota, C., Carraminana, J. J., Burillo, J., & Herrera, A. (2004). In vitro antimicrobial activity of essential oils from aromatic plants against selected foodborne pathogens. *Journal of Food Protection*, *67*, 1252–1256.

Tang, E. S. K., Huang, M., & Lim, L. Y. (2003). Ultrasonication of chitosan and chitosan nanoparticles. *International Journal of Pharmaceutics*, *265*, 103–114.

Trapani, A., De Giglio, E., Cafagna, D., Denora, N., Agrimi, G., Cassano, T., et al. (2011). Characterization and evaluation of chitosan nanoparticles for dopamine brain delivery. *International Journal of Pharmaceutics*, *419*, 296–307.

Wang, L. Y., Gu, Y. H., Zhou, Q. Z., Ma, G. H., Wan, Y. H., & Su, Z. G. (2006). Preparation and characterization of uniform-sized chitosan microspheres containing insulin by membrane emulsification and a two-step solidification process. *Colloids and Surfaces B: Biointerfaces*, *50*, 126–135.

Weiss, J., Gaysinksy, S., Davidson, M., & McClements, J. (2009). Nanostructured encapsulation systems: Food antimicrobials. In G. V. Barbosa-Cánovas, A. Mortimer, D. Lineback, W. Spiess, & K. Buckle (Eds.), *IUFoST world congress book: Global issues in food science and technology* (pp. 425–479). Amsterdam: Elsevier Inc.

Xu, Y., & Du, Y. (2003). Effect of molecular structure of chitosan on protein delivery properties of chitosan nanoparticles. *International Journal of Pharmaceutics*, *250*, 215–226.

Yang, S. J., Lin, F. H., Tsai, H. M., Lin, C. F., Chin, H. C., Wong, J. M., et al. (2011). Alginate–folic acid-modified chitosan nanoparticles for photodynamic detection of intestinal neoplasms. *Biomaterials*, *32*, 2174–2182.

Yoksan, R., Jirawutthiwongchai, J., & Arpo, K. (2010). Encapsulation of ascorbyl palmitate in chitosan nanoparticles by oil-in-water emulsion and ionic gelation processes. *Colloids and Surfaces B: Biointerfaces*, *76*, 292–297.